Surface and volume plasmons in metallic nanospheres in a semiclassical RPA-type approach: Near-field coupling of surface plasmons with the semiconductor substrate

J. Jacak,[1] J. Krasnyj,[1,2] W. Jacak,[1] R. Gonczarek,[1] A. Chepok,[2] and L. Jacak[1]
[1]*Institute of Physics, Wrocław University of Technology, Wyb. Wyspiańskiego 27, 50-370 Wrocław, Poland*
[2]*Group of Theor. Physics, International University, Fontanskaya Doroga 33, Odessa, Ukraine*
(Received 11 July 2009; revised manuscript received 15 June 2010; published 15 July 2010)

A random-phase-approximation semiclassical scheme for the description of plasmon excitations in large metallic nanospheres, with a radius range of 10–60 nm, is developed in an all-analytical version, with inclusion of irradiation phenomena. The spectrum of plasmons is determined for both surface- and volume-type excitations. The various channels for the damping of surface plasmons are evaluated and a predominant role of the irradiation losses is indicated for large metallic nanospheres, with radius greater than 10 nm. The damping-caused plasmon resonance shifts are compared with the experimental data for metallic nanoparticles of different sizes located in a dielectric medium or on the semiconductor substrate. The strong enhancement of energy transfer from the surface plasmon oscillations to the semiconductor substrate is explained in the regime of a near-field coupling of surface plasmons with semiconductor electrons in agreement with recent experimental observations for metallically surface-nanomodified photodiode systems.

DOI: 10.1103/PhysRevB.82.035418 PACS number(s): 73.21.−b, 36.40.Gk, 73.20.Mf, 78.67.Bf

I. INTRODUCTION

Rapid progress in plasmonics[1] (taking advantage of peculiar properties of plasmon polaritons[2] in nanostructured metallic interfaces) and plasmonic applications in photonics and microelectronics[3] have focused attention on metallically modified systems in nanoscale and on collective excitations of metallic plasma in a confined geometry. Of particular interest are the recently reported experimental data on giant enhancement of photoluminescence and absorption of light by semiconductor surfaces (of photodiodes) covered with metallic (gold, silver, or copper) nanospheres with sphere radii of the order of several to several tens of nanometers.[4–9] These phenomena are recognized as promising for the enhancement of the efficiency of solar cells by the application of special metallic nanoparticle coverings of photoactive layers.[4,5] Metallic nanospheres (or nanoparticles of other shape) can act as light converters, collecting energy of incident photons in surface plasmon oscillations. This energy can be next transferred to the semiconductor substrate in a more efficient manner in comparison to the direct photoeffect.

The experimental observations[4–9] suggest that the short range coupling between plasmons in nanospheres and electrons in the semiconductor substrate allows for significant growth of selective light energy transformation into a photocurrent in the diode system. This phenomenon is not described in detail as of yet; moreover, some competitive mechanisms apparently contribute, manifesting themselves in the strong sensitivity of the effect to the size and shape of the metallic nanocomponents, the type of the material and the dielectric coverings of the nanoparticles.[9,10] Nevertheless, one can argue generally that due to the nanoscale size of the metallic components, the momentum is not conserved, which leads to the allowance of all indirect optical interband transitions in the semiconductor layer, resulting in enhancement of the photocurrent in comparison to the ordinary photoeffect when only direct interband transitions are admitted.

Since the surface plasmons play a central role in the metallically modified photocell structures, the recognition of these excitations in nanoparticles is important. The surface plasmons were originally considered by Mie,[11] who provided a classical description of oscillations of electrical charge on the surface of the metallic sphere within the electron-gas model. The classical Mie frequencies are not dependent on the sphere radius, in contrast to the experimental observations for both small metallic clusters and larger spheres.

Plasmon excitations in small metallic clusters have been the subject of wide analyses[12–20] within various attitudes taking into account quantum effects. There were mostly numerical calculations "*ab initio*," including the shell-model and the Kohn-Sham "local density approximation," similar to that applied in chemistry for large molecule calculations, limited, however, to a few hundreds of electrons.[12,14–16,18] In description of metallic clusters the "jellium" model was commonly adopted, allowing for an adiabatic approach to the background ion system. In the jellium model, all the kinetics concerns the electron liquid screened by the static and uniform positive background of the ions.[12,21–23] Also variational methods for energy density and the random-phase-approximation (RPA) numerical summations (e.g., for clusters of Na with radius ~ 1 nm) (Ref. 24) as well as various semiclassical expansion methods[13,16,17] were applied. The emerging of the Mie response from the more general behavior was presented.[12,14,24] Numerical analyses using time-dependent local density approximation (TDLDA), widely applied to small clusters up to $N=200$ (e.g., Refs 12, 14, and 16), revealed the redshift of Mie resonance mainly due to so-called spill-out of the electron cloud beyond the jellium rim.

The problem of plasmon oscillations in metallic clusters was also analyzed employing analytical formulations of the Thomas-Fermi-type approach (e.g., by Kresin[13] or more recently within semiclassical expansion and the separation of mass center and relative electron dynamics[16]) but without, however, including the damping of surface plasmon oscilla-

tions due to radiation losses and addressing rather small systems (up to approximately 200 atoms, i.e., at most 2.5 nm for the radius[16]). For small clusters the damping of surface plasmons due to scattering and the decay into particle-hole pairs (Landau damping) were included,[15,17] both important rather for small clusters (scattering-induced resonance shift scales as inverse of radius and Landau damping is limited to a radius range up to 2.5 nm).[16,17]

In the range of cluster dimensions 1–2 nm the experimentally observed redshift of Mie frequency was described mainly by the spill-out effect (with corrections due to the scattering and Landau damping), which is pronounced in small nanocrystals and causes a redshift due to reducing of the electron density (Mie frequency is proportional to the square of the density).[13,14,16] However, for dimensions above only a few nanometers, the lowering of electron density caused by spill-out is on the order of single percent or smaller[13] and thus for higher nanosphere dimensions (on the order of a few tens of nm) is unimportant (the resonance frequency shift caused by spill-out is proportional to the inverse radius of a metallic sphere, as a surface-type effect, and thus diminishes with radius growth). In large nanospheres experimentally observed redshift of resonance is far bigger than this one which would correspond to spill-out including scattering and Landau damping and, moreover, significantly grows with nanoparticle size,[7] oppositely to redshift for small clusters. Thus other effects should be taken into account and their identification and explanation of different behavior patterns of plasmon resonance in large nanospheres is a purpose of the present paper.

The other quantum effects, such as magic electron numbers, related with closed shells for a confined system[13,14] also correspond to small clusters (for review cf. Ref. 12). Due to shell effect for ultrasmall clusters electron collective excitations are strongly coupled between volume and surface and also with background ionic system oscillations. The emerging of a well-formed volume plasmon for ~ 0.5 nm radius was demonstrated,[12,14] while for smaller clusters, the separation of surface and volume excitations is impossible (calculations were ranged to $l=1$ dipole mode[14]). With the growth of the cluster radius the situation changes and both types of collective excitations (translational and compressional, addressed to surface and volume oscillations, respectively) can be separated (they finally have strongly different frequencies). For nanosphere radii >10 nm one can thus safely assume that the surface and volume plasmon modes are decoupled and well defined. Note, that useful notions of volume and surface oscillations were also applied in the case of nuclear matter vibrations of compressional type[25,26] and of translational type,[27] respectively, which were then important in understanding of the giant nuclear dipole resonance experiments.

In the present paper we develop the RPA semiclassical method, originally formulated by Bohm and Pines for bulk metal,[28,29] in order to describe electron collective excitations in large metallic nanospheres, with a radius range of 10–60 nm (much larger than the Thomas-Fermi radius being on the order of interparticle separation), including both volume and surface types of plasmons in the framework of an all-analytical calculus. We pay a special attention to inclusion of radiation losses and resulting plasmon damping, which turns out to be a predominant mechanism of resonance shift in the case of large nanosphere size. This is beyond the other RPA semiclassical analyses previously addressed rather to smaller clusters, for which irradiation effects were unimportant.[13]

In the next section, the RPA equations for a local electron density are derived, including conditions imposed by the finite geometry of the nanosphere (for particularities of the solution method cf. also Ref. 30). The metal is assumed as a so-called "simple metal," i.e., allowing for the description of the electron-ion interaction by a local and not strong pseudopotential (this condition is satisfied, e.g., for noble, alkali, or transition metals).[28] In the following section, the spectra of surface and volume plasmons for the metallic nanosphere are presented, along with their modifications by the dielectric medium in which the metallic sphere can be embedded. The *e-m* response of the dielectric medium with metallic nanosphere subsystem is analyzed in the case of the dipole type ($l=1$) excitation, including modifications caused by irradiation-induced plasmon damping, resulting in a strong dependence of the resonance energy shift on the nanosphere radius, as was experimentally observed for large nanospheres.[7] Various channels of plasmon damping are considered, including radiation losses in far-field and near-field regimes (with calculus particularities shifted to Appendices A and B, respectively), and the resulting resonant spectrum modification is compared with experimentally measured dependence of emission and absorption rates on the sphere radius[7] and dielectric coating.[9,10] The giant strengthening of a coupling in the near-field regime of surface plasmons with a semiconductor substrate is described in agreement with the experimental data for the enhancement of a photocurrent in metallically nanomodified diode systems.[4–9]

II. RPA SEMICLASSICAL APPROACH TO ELECTRON DISTRIBUTION IN A METALLIC NANOSPHERE

A. Derivation of RPA equation for local electron density in a confined geometry

Let us consider a metallic sphere with radius a located in a vacuum, $\varepsilon=1$, $\mu=1$. We assume that the interaction between electrons and ions is described by a local and weak pseudopotential (this condition corresponds to the so-called simple metal case),[28] as e.g., for noble metals; of a particular significance are gold, silver, and also copper nanoparticles due to the strong visible-light plasmon resonances in these materials. The Hamiltonian for this system has the form

$$\hat{H} = -\sum_{\nu=1}^{N} \frac{\hbar^2 \nabla_\nu^2}{2M} + \frac{1}{2}\sum_{\nu\neq\nu'} u(\boldsymbol{R}_\nu - \boldsymbol{R}_{\nu'}) - \sum_{j=1}^{N_e} \frac{\hbar^2 \nabla_j^2}{2m} + \frac{1}{2}\sum_{j\neq j'} \frac{e^2}{|\boldsymbol{r}_j - \boldsymbol{r}_{j'}|} + \sum_{\nu,j} w(\boldsymbol{R}_\nu - \boldsymbol{r}_j), \tag{1}$$

where $\boldsymbol{R}_\nu$, $\boldsymbol{r}_j$ and M, m are the positions and masses of the ions and electrons, respectively; N is the number of ions in the sphere, $N_e=ZN$ is the number of collective electrons, $u(\boldsymbol{R}_\nu-\boldsymbol{R}_{\nu'})$ is the interaction of ions (ion is treated as a nucleus with electron core of closed shells), and $w(\boldsymbol{R}_\nu-\boldsymbol{r}_j)$ is

the local pseudopotential of electron-ion interaction. Assuming the jellium model[12,21,22] one can write for the background ion charge uniformly distributed over the sphere: $n_e(\boldsymbol{r}) = n_e\Theta(a-r)$, where $n_e = N_e/V$ and $n_e|e|$ is the averaged positive charge density, $V = \frac{4\pi a^3}{3}$ is the sphere volume, and Θ is the Heaviside step function. Then, neglecting ion dynamics and small electron-ion pseudopotential (shifted by jellium and electron interaction), the collective electrons can be described by the Hamiltonian

$$\hat{H}_e = \sum_{j=1}^{N_e}\left[-\frac{\hbar^2\nabla_j^2}{2m} - e^2\int\frac{n_e(\boldsymbol{r})d^3\boldsymbol{r}}{|\boldsymbol{r}_j-\boldsymbol{r}|}\right] + \frac{1}{2}\sum_{j\neq j'}\frac{e^2}{|\boldsymbol{r}_j-\boldsymbol{r}_{j'}|} \quad (2)$$

with corresponding electron wave function $\Psi_e(t)$.

A local electron density can be written as follows:[28,29]

$$\rho(\boldsymbol{r},t) = \langle\Psi_e(t)|\sum_j \delta(\boldsymbol{r}-\boldsymbol{r}_j)|\Psi_e(t)\rangle \quad (3)$$

with the Fourier picture

$$\tilde{\rho}(\boldsymbol{k},t) = \int \rho(\boldsymbol{r},t)e^{-i\boldsymbol{k}\cdot\boldsymbol{r}}d^3r = \langle\Psi_e(t)|\hat{\rho}(\boldsymbol{k})|\Psi_e(t)\rangle, \quad (4)$$

where the "operator" $\hat{\rho}(\boldsymbol{k}) = \Sigma_j e^{-i\boldsymbol{k}\cdot\boldsymbol{r}_j}$.

Using the above notation one can rewrite $\hat{H}_e$ in the following form, in an analogy to the bulk case:[28,29]

$$\hat{H}_e = \sum_{j=1}^{N_e}\left[-\frac{\hbar^2\nabla_j^2}{2m}\right] - \frac{e^2}{(2\pi)^3}\int d^3k\tilde{n}_e(\boldsymbol{k})\frac{2\pi}{k^2}[\hat{\rho}^+(\boldsymbol{k}) + \hat{\rho}(\boldsymbol{k})] + \frac{e^2}{(2\pi)^3}\int d^3k\frac{2\pi}{k^2}[\hat{\rho}^+(\boldsymbol{k})\hat{\rho}(\boldsymbol{k}) - N_e], \quad (5)$$

where: $\tilde{n}_e(\boldsymbol{k}) = \int d^3r n_e(\boldsymbol{r})e^{-i\boldsymbol{k}\cdot\boldsymbol{r}}$ and $\frac{4\pi}{k^2} = \int d^3r\frac{1}{r}e^{-i\boldsymbol{k}\cdot\boldsymbol{r}}$.

Utilizing this form of the electron Hamiltonian one can write out

$$\frac{d^2\hat{\rho}(\boldsymbol{k})}{dt^2} = \frac{1}{(i\hbar)^2}\{[\hat{\rho}(\boldsymbol{k}),\hat{H}_e],\hat{H}_e\} \quad (6)$$

in the following form:

$$\frac{d^2\hat{\rho}(\boldsymbol{k})}{dt^2} = -\sum_j e^{-i\boldsymbol{k}\cdot\boldsymbol{r}_j}\left\{-\frac{\hbar^2}{m^2}(\boldsymbol{k}\cdot\nabla_j)^2 + \frac{\hbar^2k^2}{m^2}i\boldsymbol{k}\cdot\nabla_j + \frac{\hbar^2k^4}{4m^2}\right\} - \frac{4\pi e^2}{m(2\pi)^3}\int d^3q\tilde{n}_e(\boldsymbol{q})\frac{\boldsymbol{k}\cdot\boldsymbol{q}}{q^2}\hat{\rho}(\boldsymbol{k}-\boldsymbol{q}) - \frac{4\pi e^2}{m(2\pi)^3}\int d^3q\hat{\rho}(\boldsymbol{k}-\boldsymbol{q})\frac{\boldsymbol{k}\cdot\boldsymbol{q}}{q^2}\hat{\rho}(\boldsymbol{q}). \quad (7)$$

If one takes into account that $\hat{\rho}(\boldsymbol{k}-\boldsymbol{q})\hat{\rho}(\boldsymbol{q}) = \delta\hat{\rho}(\boldsymbol{k}-\boldsymbol{q})\delta\hat{\rho}(\boldsymbol{q}) + \tilde{n}_e(\boldsymbol{k}-\boldsymbol{q})\delta\hat{\rho}(\boldsymbol{q}) + \delta\hat{\rho}(\boldsymbol{k}-\boldsymbol{q})\tilde{n}_e(\boldsymbol{q}) + \tilde{n}_e(\boldsymbol{k}-\boldsymbol{q})\tilde{n}_e(\boldsymbol{q})$ and $\tilde{n}_e(\boldsymbol{q})\hat{\rho}(\boldsymbol{k}-\boldsymbol{q}) = \tilde{n}_e(\boldsymbol{q})\delta\hat{\rho}(\boldsymbol{k}-\boldsymbol{q}) + \tilde{n}_e(\boldsymbol{q})\tilde{n}_e(\boldsymbol{k}-\boldsymbol{q})$, where $\delta\hat{\rho}(\boldsymbol{k}) = \hat{\rho}(\boldsymbol{k}) - \tilde{n}_e(\boldsymbol{k})$ describes the operator of local electron density fluctuations above the uniform distribution, one can rewrite Eq. (7) in the form

$$\frac{d^2\delta\hat{\rho}(\boldsymbol{k})}{dt^2} = -\sum_j e^{-i\boldsymbol{k}\cdot\boldsymbol{r}_j}\left\{-\frac{\hbar^2}{m^2}(\boldsymbol{k}\cdot\nabla_j)^2 + \frac{\hbar^2k^2}{m^2}i\boldsymbol{k}\cdot\nabla_j + \frac{\hbar^2k^4}{4m^2}\right\} - \frac{4\pi e^2}{m(2\pi)^3}\int d^3q\tilde{n}_e(\boldsymbol{k}-\boldsymbol{q})\frac{\boldsymbol{k}\cdot\boldsymbol{q}}{q^2}\delta\hat{\rho}(\boldsymbol{q}) - \frac{4\pi e^2}{m(2\pi)^3}\int d^3q\,\delta\hat{\rho}(\boldsymbol{k}-\boldsymbol{q})\frac{\boldsymbol{k}\cdot\boldsymbol{q}}{q^2}\delta\hat{\rho}(\boldsymbol{q}). \quad (8)$$

Thus for the electron density fluctuation, $\delta\tilde{\rho}(\boldsymbol{k},t) = \langle\Psi_e|\delta\hat{\rho}(\boldsymbol{k},t)|\Psi_e\rangle = \tilde{\rho}(\boldsymbol{k},t) - \tilde{n}_e(\boldsymbol{k})$, we find

$$\frac{\partial^2\delta\tilde{\rho}(\boldsymbol{k},t)}{\partial t^2} = -\langle\Psi_e|\sum_j e^{-i\boldsymbol{k}\cdot\boldsymbol{r}_j}\left\{-\frac{\hbar^2}{m^2}(\boldsymbol{k}\cdot\nabla_j)^2 + \frac{\hbar^2k^2}{m^2}i\boldsymbol{k}\cdot\nabla_j + \frac{\hbar^2k^4}{4m^2}\right\}|\Psi_e\rangle - \frac{4\pi e^2}{m(2\pi)^3}\int d^3q\tilde{n}_e(\boldsymbol{k}-\boldsymbol{q})\times\frac{\boldsymbol{k}\cdot\boldsymbol{q}}{q^2}\delta\tilde{\rho}(\boldsymbol{q},t) - \frac{4\pi e^2}{m(2\pi)^3}\int d^3q\frac{\boldsymbol{k}\cdot\boldsymbol{q}}{q^2}\times\langle\Psi_e|\delta\hat{\rho}(\boldsymbol{k}-\boldsymbol{q})\delta\hat{\rho}(\boldsymbol{q})|\Psi_e\rangle. \quad (9)$$

Within the semiclassical approximation three components of the first term on the right-hand side of Eq. (9) can be estimated as: $k^2v_F^2\delta\tilde{\rho}(\boldsymbol{k},t)$, $k^3v_F/k_T\delta\tilde{\rho}(\boldsymbol{k},t)$, and $k^4v_F^2/k_T^2\delta\tilde{\rho}(\boldsymbol{k},t)$, respectively ($1/k_T$ is the Thomas-Fermi radius,[28] $k_T = \sqrt{\frac{6\pi n_e e^2}{\epsilon_F}}$, ϵ_F is the Fermi energy, and v_F is the Fermi velocity). The contributions of the second and third components of the first term can be neglected in comparison to the first component. Small and thus negligible is also the third term in the right-hand side of Eq. (9), as involving a product of two $\delta\tilde{\rho}$ (which we assumed small, $\delta\tilde{\rho}/n_e \ll 1$). This approach corresponds to the RPA attitude formulated for bulk metal[28,29] [note that $\delta\hat{\rho}(0) = 0$ and the coherent RPA contribution of interaction is comprised by the last but one term in Eq. (9)].

Within the RPA, Eq. (9) thus attains the form

$$\frac{\partial^2\delta\tilde{\rho}(\boldsymbol{k},t)}{\partial t^2} = \frac{2k^2}{3m}\langle\Psi_e|\sum_j e^{-i\boldsymbol{k}\cdot\boldsymbol{r}_j}\frac{\hbar^2\nabla_j^2}{2m}|\Psi_e\rangle - \frac{4\pi e^2}{m(2\pi)^3}\times\int d^3q\tilde{n}_e(\boldsymbol{k}-\boldsymbol{q})\frac{\boldsymbol{k}\cdot\boldsymbol{q}}{q^2}\delta\tilde{\rho}(\boldsymbol{q},t), \quad (10)$$

where for the case of spherical symmetry

$$\langle\Psi_e|\sum_j e^{-i\boldsymbol{k}\cdot\boldsymbol{r}_j}\frac{\hbar^2}{m^2}(\boldsymbol{k}\cdot\nabla_j)^2|\Psi_e\rangle \simeq \frac{2k^2}{3m}\langle\Psi_e|\sum_j e^{-i\boldsymbol{k}\cdot\boldsymbol{r}_j}\frac{\hbar^2\nabla_j^2}{2m}|\Psi_e\rangle.$$

In the position representation Eq. (10) can be rewritten in the following manner:

$$\frac{\partial^2\delta\tilde{\rho}(\boldsymbol{r},t)}{\partial t^2} = -\frac{2}{3m}\nabla^2\langle\Psi_e|\sum_j\delta(\boldsymbol{r}-\boldsymbol{r}_j)\frac{\hbar^2\nabla_j^2}{2m}|\Psi_e\rangle + \frac{\omega_p^2}{4\pi}\nabla\times\left\{\Theta(a-r)\nabla\int d^3r_1\frac{1}{|\boldsymbol{r}-\boldsymbol{r}_1|}\delta\tilde{\rho}(\boldsymbol{r}_1,t)\right\}. \quad (11)$$

The Thomas-Fermi averaged kinetic energy can be represented as follows:[28]

$$\langle \Psi_e | - \sum_j \delta(\boldsymbol{r}-\boldsymbol{r}_j)\frac{\hbar^2\nabla_j^2}{2m}|\Psi_e\rangle$$
$$\simeq \frac{3}{5}(3\pi^2)^{2/3}\frac{\hbar^2}{2m}[\rho(\boldsymbol{r},t)]^{5/3}$$
$$= \frac{3}{5}(3\pi^2)^{2/3}\frac{\hbar^2}{2m}n_e^{5/3}\Theta(a-r)\left[1+\frac{5}{3}\frac{\delta\tilde{\rho}(\boldsymbol{r},t)}{n_e}+\ldots\right]. \quad (12)$$

Note that here neglected gradient terms [in particular, the von Weizsäcker term, $\sim(\nabla\rho)^2/(4\rho)$, beyond the Thomas-Fermi formula for kinetic-energy functional $\sim\rho^{5/3}$][12] strongly affect the finite system properties especially of small metallic clusters. The contribution of this particular term (von Weizsäcker) depends on the approximation in various versions of corrections to the Thomas-Fermi approach[13] (the coefficient of von Weizsäcker term is treated even as a convenient fitting parameter). The gradient terms are included, in an inexplicit manner, in TDLDA-type methods based on the Kohn-Sham equation. As follows from the respective analyses, the contributions related to these terms (mostly the spill-out effect) are more important for small clusters (when the surface dominates) and gradually diminish with the growth of the nanosphere radius.[12–14,16,17]

Taking then into account that $\nabla\Theta(a-r)=-\frac{\boldsymbol{r}}{r}\delta(a-r)$, one can rewrite Eq. (11) in the following manner:

$$\frac{\partial^2\delta\tilde{\rho}(\boldsymbol{r},t)}{\partial t^2} = \left[\frac{2}{3}\frac{\epsilon_F}{m}\nabla^2\delta\tilde{\rho}(\boldsymbol{r},t)-\omega_p^2\delta\tilde{\rho}(\boldsymbol{r},t)\right]\Theta(a-r)$$
$$-\frac{2}{3m}\nabla\left\{\left[\frac{3}{5}\epsilon_F n_e+\epsilon_F\delta\tilde{\rho}(\boldsymbol{r},t)\right]\frac{\boldsymbol{r}}{r}\delta(a-r)\right\}$$
$$-\left[\frac{2}{3}\frac{\epsilon_F}{m}\frac{\boldsymbol{r}}{r}\nabla\,\delta\tilde{\rho}(\boldsymbol{r},t)\right.$$
$$\left.+\frac{\omega_p^2}{4\pi}\frac{\boldsymbol{r}}{r}\nabla\int d^3r_1\frac{1}{|\boldsymbol{r}-\boldsymbol{r}_1|}\delta\tilde{\rho}(\boldsymbol{r}_1,t)\right]\delta(a-r). \quad (13)$$

In the above formula ω_p is the bulk plasmon frequency, $\omega_p^2=\frac{4\pi n_e e^2}{m}$. The solution of Eq. (13) can be decomposed into two parts related to the distinct domains

$$\delta\tilde{\rho}(\boldsymbol{r},t)=\begin{cases}\delta\tilde{\rho}_1(\boldsymbol{r},t) & \text{for } r<a\\ \delta\tilde{\rho}_2(\boldsymbol{r},t) & \text{for } r\geq a,\ (r\to a+)\end{cases} \quad (14)$$

corresponding to the volume and surface excitations, respectively. These two parts of local electron-density fluctuations satisfy the equations [according to Eq. (13)]

$$\frac{\partial^2\delta\tilde{\rho}_1(\boldsymbol{r},t)}{\partial t^2}=\frac{2}{3}\frac{\epsilon_F}{m}\nabla^2\delta\tilde{\rho}_1(\boldsymbol{r},t)-\omega_p^2\delta\tilde{\rho}_1(\boldsymbol{r},t) \quad (15)$$

and (here $\epsilon=0+$)

$$\frac{\partial^2\delta\tilde{\rho}_2(\boldsymbol{r},t)}{\partial t^2}=-\frac{2}{3m}\nabla\left\{\left[\frac{3}{5}\epsilon_F n_e+\epsilon_F\delta\tilde{\rho}_2(\boldsymbol{r},t)\right]\frac{\mathbf{r}}{r}\delta(a+\epsilon-r)\right\}$$
$$-\left[\frac{2}{3}\frac{\epsilon_F}{m}\frac{\boldsymbol{r}}{r}\nabla\,\delta\tilde{\rho}_2(\boldsymbol{r},t)\right.$$
$$+\frac{\omega_p^2}{4\pi}\frac{\boldsymbol{r}}{r}\nabla\int d^3r_1\frac{1}{|\boldsymbol{r}-\boldsymbol{r}_1|}(\delta\tilde{\rho}_1(\boldsymbol{r}_1,t)\Theta(a-r_1)$$
$$\left.+\delta\tilde{\rho}_2(\boldsymbol{r}_1,t)\Theta(r_1-a))\right]\delta(a+\epsilon-r). \quad (16)$$

The Dirac delta in Eq. (13) results due to the derivative of the Heaviside step function—ideal jellium charge distribution. In Eq. (16) an infinitesimal shift, $\epsilon=0+$, is introduced to fulfill requirements of the distribution delta definition (its singular point has to be an inner point of an open subset of the domain). This shift is only of a formal character and does not reflect any asymmetry. Some kind of asymmetry is, however, caused by the last term in Eq. (13), the gradient-type term, which describes the electric field induced by electron fluctuations. The electric field due to surface charges is zero inside the sphere and therefore cannot influence the volume excitations. Oppositely, the volume charge fluctuation-induced electric field can excite the surface fluctuations. This asymmetry is visible by comparison of Eqs. (15) and (16), for volume and surface plasmons, respectively.

In the semiclassical approach the domain of the surface charge fluctuations is extremely narrow (surface only). For the fuzzy surface, as for small clusters with spill-out, the surface charge fluctuations encompass a widened domain below and above the jellium rim. This results in mutual coupling of volume and surface plasmons in ultrasmall clusters ($N<60$).[12,14] Within the semiclassical approach, volume plasmons described by Eq. (15) are independent of the surface plasmons, though the latter can be excited by the former ones, due to the last term in Eq. (16) (which is caused by electric field induced by volume charge fluctuations, while oppositely, surface charge oscillations do not influence inside of the sphere). This expresses a coupling between surface and volume plasmons in large metallic nanospheres within the semiclassical RPA approach.

B. Solution of RPA equations: Volume and surface plasmon frequencies

Equations (15) and (16) can be solved upon imposed boundary and symmetry conditions. Let us represent both parts of the electron fluctuation in the following manner:

$$\delta\tilde{\rho}_1(\boldsymbol{r},t)=n_e[f_1(r)+F(\boldsymbol{r},t)],\quad \text{for } r<a,$$
$$\delta\tilde{\rho}_2(\boldsymbol{r},t)=n_e f_2(r)+\sigma(\Omega,t)\delta(r+\epsilon-a),\quad \epsilon=0+,$$
$$\text{for } r\geq a,\quad (r\to a+) \quad (17)$$

and now let us choose the convenient initial conditions, $F(\boldsymbol{r},t)|_{t=0}=0$, $\sigma(\Omega,t)|_{t=0}=0$, ($\Omega$ is the spherical angle), moreover $[1+f_1(r)]|_{r=a}=f_2(r)|_{r=a}$ (continuity condition), $F(\boldsymbol{r},t)|_{r\to a}=0$, $\int\rho(\boldsymbol{r},t)d^3r=N_e$ (neutrality condition).

We arrive[30] thus with the explicit form of the solutions of Eqs. (15) and (16)

$$f_1(r) = -\frac{k_T a + 1}{2} e^{-k_T(a-r)} \frac{1 - e^{-2k_T r}}{k_T r}, \quad \text{for} \quad r < a,$$

$$f_2(r) = \left[k_T a - \frac{k_T a + 1}{2}(1 - e^{-2k_T a}) \right] \frac{e^{-k_T(r-a)}}{k_T r}, \quad \text{for} \quad r \geq a, \tag{18}$$

where $k_T = \sqrt{\frac{6\pi n_e e^2}{\epsilon_F}} = \sqrt{\frac{3\omega_p^2}{v_F^2}}$. For the time-dependent parts of the electron fluctuations we find

$$F(\mathbf{r},t) = \sum_{l=1}^{\infty} \sum_{m=-l}^{l} \sum_{n=1}^{\infty} A_{lmn} j_l(k_{nl} r) Y_{lm}(\Omega) \sin(\omega_{nl} t) \tag{19}$$

and

$$\sigma(\Omega,t) = \sum_{l=1}^{\infty} \sum_{m=-l}^{l} \frac{B_{lm}}{a^2} Y_{lm}(\Omega) \sin(\omega_{0l} t) + \sum_{l=1}^{\infty} \sum_{m=-l}^{l} \sum_{n=1}^{\infty} A_{lmn} \frac{(l+1)\omega_p^2}{l\omega_p^2 - (2l+1)\omega_{nl}^2} Y_{lm}(\Omega) n_e \times \int_0^a dr_1 \frac{r_1^{l+2}}{a^{l+2}} j_l(k_{nl} r_1) \sin(\omega_{nl} t), \tag{20}$$

where $j_l(\xi) = \sqrt{\frac{\pi}{2\xi}} I_{l+1/2}(\xi)$ is the spherical Bessel function, $Y_{lm}(\Omega)$ is the spherical function, $\omega_{nl} = \omega_p \sqrt{1 + \frac{x_{nl}^2}{k_T^2 a^2}}$ are the frequencies of electron volume self-oscillations (volume plasmon frequencies), x_{nl} are the nodes of the Bessel function $j_l(\xi)$, and $k_{nl} = x_{nl}/a$ and $\omega_{0l} = \omega_p \sqrt{\frac{l}{2l+1}}$ are the frequencies of electron surface self-oscillations (surface plasmon frequencies).

From the above equations it follows thus that the local electron density (within RPA attitude) has the form

$$\rho(\mathbf{r},t) = \rho_0(r) + \rho_{neq}(\mathbf{r},t), \tag{21}$$

where the RPA equilibrium electron distribution is (correcting the uniform distribution n_e)

$$\rho_0(r) = \begin{cases} n_e[1 + f_1(r)] & \text{for } r < a \\ n_e f_2(r) & \text{for } r \geq a, \quad r \to a+ \end{cases} \tag{22}$$

and the nonequilibrium, of plasmon oscillation type, is

$$\rho_{neq}(\mathbf{r},t) = \begin{cases} n_e F(\mathbf{r},t) & \text{for } r < a \\ \sigma(\Omega,t)\delta(a + \epsilon - r) & \epsilon = 0+, \text{ for } r \geq a, \quad r \to a+. \end{cases} \tag{23}$$

The function $F(\mathbf{r},t)$ displays volume plasmon oscillations while $\sigma(\Omega,t)$ describes the surface plasmon oscillations. Let us emphasize that in the formula for $\sigma(\Omega,t)$, Eq. (20), the first term corresponds to surface self-oscillations, while the second term describes the surface oscillations induced by the volume plasmons. The frequencies of the surface self-oscillations are

$$\omega_{0l} = \omega_p \sqrt{\frac{l}{2l+1}}, \tag{24}$$

which, for $l=1$, agrees with the dipole-type surface oscillations described originally by Mie,[11] $\omega_{01} = \omega_p/\sqrt{3}$.

In order to account for the influence of dielectric surroundings on the surface plasmons in the metallic nanosphere, let us assume that electrons on the surface ($r=a+$, i.e., $r \geq a$, $r \to a$) interact with Coulomb forces renormalized by the relative dielectric constant $\varepsilon > 1$. Thus instead of Eq. (16) one can consider its modification with the factor $\frac{1}{\varepsilon}$ in the last its term [Eq. (15) remains unchanged]. The solution of such modified equation is of the same form as that for the Eq. (16) case but it has the new surface plasmon frequencies

$$\omega_{0l} = \omega_p \sqrt{\frac{l}{2l+1}\frac{1}{\varepsilon}}. \tag{25}$$

The frequency of surface electron self-oscillations, changed by the factor $\sqrt{\frac{1}{\varepsilon}}$, can be reduced significantly in comparison to the vacuum case, as in many materials ε is relatively big (ε corresponds to its high-frequency limiting value, the same one that is involved in a refraction coefficient). This surface plasmon frequency given by Eq. (25) does not reproduce, for the dipole case $l=1$, the classical Mie formula,[19,22,31] $\omega_p \frac{1}{\sqrt{2\varepsilon+1}}$. It is lower than the Mie one, which corresponds, to some extent, with the data indicated in Fig. 3 in Ref. 19, in which there are presented resonance frequencies obtained within a more thorough (TDLDA) method for potassium clusters (with $N < 200$), and they are also located below corresponding classical Mie values. The red shift of TDLDA frequencies is, however, caused mainly by spill-out for ultrasmall clusters and only additionally by the dielectric constant of surrounding material (though this latter contribution is also important in comparison to classical electrostatic screening—cf. Fig. 1 in Ref. 19). For larger nanospheres (when spill-out is small) one may expect, however, the dielectric mish-mash-induced redshift to be closer to the RPA semiclassical one [Eq. (25)], as diminishing spill-out results in a narrowing domain of surface oscillations.

III. EVALUATION OF A DAMPING RATE FOR SURFACE PLASMONS

The RPA semiclassical Eqs. (15) and (16) for plasmon excitations reveal the form of the oscillator-equation type. Thus, it is easy to include, in a phenomenological manner, the attenuation of these excitations via a damping term $\frac{2}{\tau^{(i)}} \frac{\partial \rho_i(\mathbf{r},t)}{\partial t}$, which can be added to the left-hand sides of Eqs. (15) and (16) (assuming that the volume modes, $i=1$, and the surface modes, $i=2$, are damped with the attenuation times $\tau^{(i)}$, respectively). Thus, the time-dependent solution of such a modified Eq. (15) attains the form as given by Eq. (19) with the factor $e^{-t/\tau^{(1)}}$ and shifted frequency $\omega'_{nl} = \sqrt{\omega_{nl}^2 - \frac{1}{(\tau^{(1)})^2}}$, for the volume modes. Similarly for the surface plasmons [Eq. (16)], the attenuation leads to the factor

TABLE I. Comparison with experimental data (Ref. 7) for Au nanospheres in water.

Nanosphere radius	a	50 nm	40 nm	25 nm
Attenuation rate due to far-field radiation losses	$\omega_1\tau_2^{(2)}$	1.51	2.95	12.09
Shifted self-frequency rate	$\frac{\omega'}{\omega_1}=\sqrt{1-(\omega_1\tau_2^{(2)})^{-2}}$	0.75	0.94	0.99
Redshifted oscillation energy	$\hbar\omega'$ (theor.)	2.16 eV	2.70 eV	2.87 eV
Redshifted oscillation energy	$\hbar\omega'$ (exper.)	2.16 eV	2.26 eV	2.36 eV

$e^{-t/\tau^{(2)}}$ for the first part of the solution (20) [and the simultaneously shifted frequency $\omega'_{0l}=\sqrt{\omega_{0l}^2-\frac{1}{(\tau^{(2)})^2}}$] while the second term of Eq. (20) acquires an additional factor $e^{-t/\tau^{(1)}}$ [and the shifted frequency, $\omega'_{0l}=\sqrt{\omega_{nl}^2-\frac{1}{(\tau^{(1)})^2}}$].

Let us concentrate on the damping of surface plasmons described by $\frac{1}{\tau^{(2)}}$. The interaction with phonons, electrons, and lattice defects contribute to the relaxation rate $\frac{1}{\tau_1^{(2)}}$ with $\frac{1}{\tau_1^{(2)}}$, which is determined by the mean free path of electrons in the nanosphere, reduced additionally in comparison to the bulk case by inelastic scatterings with the sphere surface. One can use the estimation[32] $\frac{1}{\tau_1^{(2)}}\sim\frac{v_F}{\lambda_B}+\frac{Cv_F}{a}$, where v_F is the Fermi velocity, λ_B is an effective value of the mean-free path, C is a constant of order 1, and a is the nanosphere radius (for Ag, $v_F=1.4\times10^6$ m/s, $\lambda_B\simeq57$ nm, which for $a=25$ nm gives $\frac{1}{\tau_1^{(2)}}=8\times10^{13}$ s^{-1}, while rather a femtosecond decay time agrees with the measurements on Ag nanoparticles[33]). Note that the decomposition of surface plasmons due to the creation of particle-hole pairs (Landau damping)[15,17] is efficient only for small clusters.[17]

Another type of energy dissipation can be associated with the radiation decay. The far-field radiation (i.e., for distances much longer than the wavelength $\lambda\gg a$) gives the contribution to the relaxation $\frac{2}{\tau_2^{(2)}}\sim\frac{2e^2}{3mc^3}\omega_1^2\sim1.6\times10^8$ s^{-1} (for $\omega_1\sim5\times10^{15}$ s^{-1}) per single electron due to the Lorentz friction.[34] If one multiplies it by the electron number $N_e=\frac{4\pi a^3}{3}n_e$, $n_e=\frac{m\omega_p^2}{4\pi e^2}$ (in order to account for the probability of energy transfer from the total system), one can arrive at the value $\frac{1}{\tau_2^{(2)}}=\omega_1\frac{1}{3}(\frac{\omega_p a}{\sqrt{3}c})^3$, which dominates over $\frac{1}{\tau_1^{(2)}}$ for not too small spheres.[22,23,33] This channel of plasmon energy dissipation allows for explanation of the surface plasmon oscillations behavior with growing a (as $\frac{1}{\tau_2^{(2)}}$ scales as a^3) for nanospheres embedded in a dielectric medium (like in the water, as is presented in Table I for nanoparticles of gold). The more precise derivation of the far-field radiation losses expressed by $\frac{1}{\tau_2^{(2)}}$ is presented in Appendix A, leading to the same formula for $\frac{1}{\tau_2^{(2)}}$ as given above. Note that if the attenuation rate $\omega_1\tau_2^{(2)}$ is closer to 1, then the attenuation-induced shift of the self-frequency is greater, $\omega'=\omega_1\sqrt{1-(\omega_1\tau_2^{(2)})^{-2}}$ and this behavior coincides with the experimental observations[6,7] (for $\frac{1}{\omega_1\tau_2^{(2)}}\geq1$ the overdamped regime is attained without free plasmon oscillations).

For Au, $\hbar\omega_p=8.57$ eV and the surface plasmon energy $\hbar\omega_1=2.87$ eV. This value of $\hbar\omega_1$ is estimated assuming a coincidence of theoretically predicted self-frequency shifted by attenuation with experimentally measured values for $a=50$ nm; note that the discrepancy between the experimental redshift and the theoretical one grows for smaller a, which is probably caused by the strengthening of the impact of $\frac{1}{\tau_1^{(2)}}\sim1/a$ at smaller a, resulting in a decrease in the redshift in comparison to its value caused by $\frac{1}{\tau_2^{(2)}}\sim a^3$. This tendency at decreasing radius a seems to also be confirmed by measurements for silver clusters with small dimensions ≤10 nm, which was reported in Refs. 35 and 36.

Note that for small metallic clusters, the quantum spill-out of the electron cloud beyond positive jellium causes a redshift of resonance Mie frequency lowering, although, with radius growth (thus it is in fact a blueshift with radius growth), oppositely to the irradiation-induced shift described above for larger nanospheres. The additional effect of polarization of the ionic system (this effect is beyond the jellium model) can lead to a similar inverse frequency shift, albeit rather small. Jellium oscillation corrections (of phonon type), included in the effective time rate for damping via the effective mean-free path λ_B, are rather significant only for small systems[12,14] (for summaries of the various effects causing redshift and blueshift of resonance with radius growth, cf. also Ref. 37). Thus, for the sphere radius range, 10–60 nm, the radiation losses cause an overwhelming contribution to damping and to the resulting redshift of the surface plasmon resonance, cf. Fig. 1. In this figure the comparison of damping contributions due to the scattering effects, $\sim\frac{v_F}{\lambda_B}+\frac{v_F}{a}$ and due to the radiation losses in the dielectric surroundings, $\sim a^3$, are presented. For $a>10$ nm the latter channel clearly dominates. The radiation-caused redshift strongly grows with the radius of the nanosphere similarly as is observed in the experiment for the range of sphere radii from 25 to 50 nm (for Au).[7]

The next source of the attenuation of surface plasmons would be connected with the transport of dipole oscillation energy between nanoparticles due to the Förster-type coupling[32] in the case of sufficiently dense location of the metallic nanoparticles. Nevertheless, taking into account that for a uniform nanoparticle distribution in the dielectric medium, the same energy rates simultaneously escape and arrive at a particular nanosphere due to interactions with other nanospheres (nearest-neighbors), this coupling does not contribute to the relaxation time (at least for uniformly distributed metallic nanocomponents).

The situation significantly changes, however, if metallic nanoparticles are deposited on the surface of the semiconductor substrate. Then the near-field *e-m* energy transfer from oscillating dipoles (surface plasmons with $l=1$) to the electrons in substrate semiconductor starts to be the dominant channel of surface plasmon dissipation. The corresponding time rate can be estimated by the Fermi golden rule applied to the system of plasmons coupled in the near-field

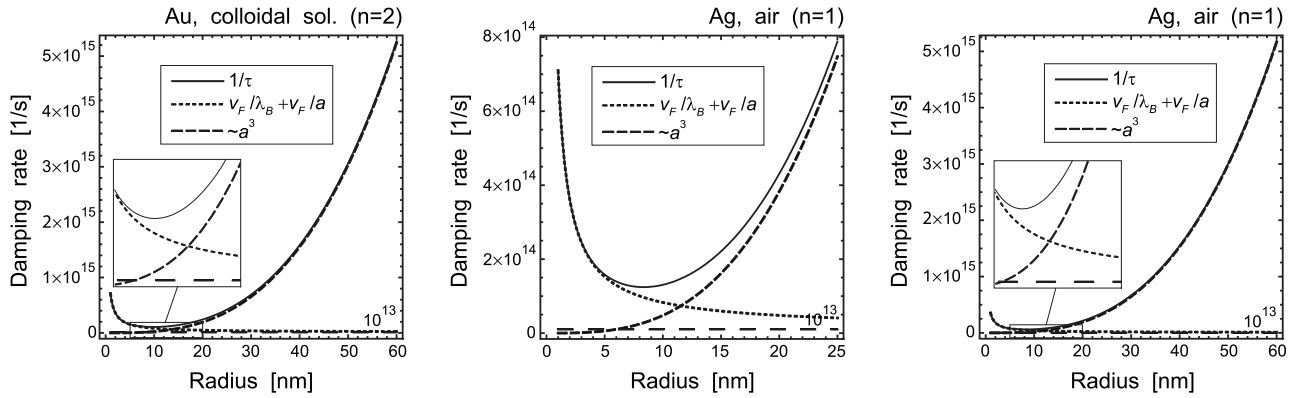

FIG. 1. Comparison of contributions to surface plasmon damping (upper curve) of the scattering term, $\sim\frac{v_F}{\lambda_B}+\frac{v_F}{a}$, and (far-field) radiation loss-induced damping, $\sim a^3$, Eq. (A10), for large metallic nanospheres (Au and Ag); for sphere radii larger than 10 nm irradiation-induced-damping dominates (horizontal dashed line indicates 10^{13} level).

zone with the semiconductor substrate. One can consider two situations: the first one, in which the external electric field is rapidly switched off, which excites surface plasmons, gradually (with lowering amplitude of oscillations) transferring next energy to the semiconductor; and the second one, in which there is a stationary state of plasmons (with constant amplitude) with a mediating role of plasmons transferring the entire energy of incident photons to the semiconductor. The latter case corresponds thus to a stationary solution of a driven and damped oscillator while the former one corresponds to free damped oscillations. In both cases the damping rate is the same, as it corresponds to the same substrate in a near-field zone. For free damped oscillations the total initial oscillation energy (assessed in Appendix A) is gradually lost with the time ratio $\frac{1}{\tau_3^{(2)}}$. This allows for calculation of the $\frac{1}{\tau_3^{(2)}}$, which is presented in Appendix B Utilizing a similar calculus as in Appendix A, one can assess the value of the corresponding damping rate $\frac{1}{\tau_3^{(2)}}$, assuming that the total energy loss of surface plasmons is transferred to the semiconductor substrate with additional renormalization by a factor β lowering an efficiency of this channel (β is a phenomenological factor introduced in order to account for the geometry-induced proximity-type constraints imposed on the dipole near-field coupling of the nanosphere with the underlying semiconductor layer). Thus, it is sufficient to calculate the energy income in the semiconductor due to the nanosphere near-field dipole coupling, as is done in Appendix B (within the Fermi golden rule scheme). For this channel of surface plasmon energy dissipation we deal with the scaling of the resonance energy shift with the dot radius, similar to that for $\frac{1}{\tau_2^{(2)}}$, however, with a possible correction induced by β dependence on a (it may be important, as for the nanosphere located on the planar semiconductor surface one can use an estimation $\beta \sim c\frac{h^2}{a^2} \sim 10^{-3}$ (for $a=50$ nm), where c is a constant and h is an effective range of near-field coupling). The parameter β significantly grows in the case when the whole nanosphere is in the near-field contact with the substrate, i.e., when the nanosphere is completely embedded in the semiconductor medium. For nanospheres deposited on the real semiconductor surface, the parameter β is obtained through fitting the experimental data (cf. Table II).

Assuming stationary conditions (i.e., constant-in-time amplitude of the surface plasmon oscillations, which corresponds to a balance of the incoming energy of incident photons with the energy outgoing to the semiconductor substrate) the relevant damping is governed by the near-field dipole interaction (for $R \ll \lambda$) expressed by the scalar potential[34] with an amplitude $D_0(\omega)$

$$\varphi(\boldsymbol{R},t) = \frac{1}{\varepsilon_0 R^2}\boldsymbol{n}\cdot\boldsymbol{D}_0(\omega)\sin(\omega t). \tag{26}$$

The matrix element of near-field dipole interaction for the transition of a semiconductor electron from the state in the valence to the conduction band, assumed as $\Psi_{i(f)}(\boldsymbol{r},t) = (2\pi)^{-3/2}\exp[i\boldsymbol{k}\cdot\boldsymbol{r} - iE_{i(f)}(\boldsymbol{k})t/\hbar]$ (i—initial and f—final, respectively) is calculated in Appendix B, [Eq. (B5)], which leads to a probability of transition per time unit,

$$\delta w = \frac{e^2[D_0(\omega)]^2\mu\sqrt{m_p^* m_n^*}}{3(4\pi^3)^2\hbar^5\varepsilon^2}(\hbar\omega - E_g),$$

where $D_0(\omega)$ is the surface plasmon dipole oscillation amplitude, adjusted to the balance of energy income and outcome

TABLE II. Comparison with the experimental data (Ref. 7) for Au nanospheres on Si layer.

a (nm)	n_s (10^8/cm^2)	x_m	$\omega_m = x_m\hbar\omega_1$ (theor) (eV)	$\hbar\omega_m$ (expt.) (eV)	$\phi(x_m)$	$\frac{I'}{I}(x_m)$
50	0.8	0.772	2.09	2.25	0.84	1.55
40	1.6	0.951	2.58	2.48	3.00	1.9
25	6.6	0.997	2.71	2.70	49.42	1.75

(via the shift of the resonance for stationary driven and damped oscillations).

Taking into account that the number of incident photons in the volume V of a semiconductor equals $\frac{\varepsilon E_0^2 V}{8\pi\hbar\omega}$ and that the volume rate of metallic components is $C_0=N_m\frac{4\pi a^3}{3V}$ (N_m—the number of nanospheres), the probability that an energy of a single incident photon is transferred to the semiconductor via surface plasmons on metallic nanoadmixtures can be expressed as [with δw given by Eq. (B5)]

$$q_m=\beta N_m\delta w\left(\frac{\varepsilon E_0^2 V}{8\pi\hbar\omega}\right)^{-1}=\frac{\beta C_0 e^2\omega f^2(\omega)a^3}{8\pi^6\hbar^4\varepsilon}\mu\sqrt{m_p^* m_n^*}(\hbar\omega-E_g),\tag{27}$$

where $f(\omega)=\frac{\omega_1^2}{\sqrt{(\omega_1^2-\omega^2)^2+4\omega^2/(\tau_3^{(2)})^2}}$ is the amplitude of forced surface plasmon oscillations.

In order to assess efficiency of the near-field coupling channel one can estimate the ratio of the probability of energy absorption in the semiconductor via mediation of surface plasmons (per single photon incident on the metallic nanospheres) to the energy attenuation in the semiconductor directly from a planar wave illumination (also per single photon). In the latter case the energy attenuation in the semiconductor per single incident photon is given by the formula for ordinary photoeffect, $q=\frac{2\sqrt{2}}{3\pi^6}\frac{e^2\mu^{5/2}}{m_p^{*2}\omega\varepsilon\hbar^3}(\hbar\omega-E_g)^{3/2}$ (cf. e.g., Ref. 38). The ratio $\frac{q_m}{q}$ turns out to be of order of $10^4\frac{\beta 40}{H[\mathrm{nm}]}$ (at a typical surface density of nanoparticles, $n_s\sim 10^8/\mathrm{cm}^2$) which (including the phenomenological factor β, and H—the semiconductor photoactive layer depth) is sufficient to explain the scale of the experimentally observed strong enhancement of absorption and emission rates. It should be noted that $\frac{1}{\tau_3^{(2)}}$ grows with β [cf. Eq. (B9)] and would attain critical value for an overdamped oscillator ($\frac{1}{\tau_3^{(2)}\omega_1}=1$), which precludes surface plasmon free oscillations.

Very high efficiency (even if decreased by β) of the near-field energy transfer from surface plasmons to the semiconductor substrate is caused mainly by a contribution of all interband transitions, not restricted here to the direct (vertical) ones as for ordinary photoeffect, due to the absence of the momentum conservation constraints for nanosystems, cf. Appendix B The strengthening of the probability transition due to all indirect interband paths of excitations in the semiconductor is probably responsible for the observed experimentally strong enhancement of light absorption and emission in diode systems mediated by surface plasmons in nanoparticle surface coverings.[4–9]

In the balanced state of the system when the incoming energy of light is transferred to the semiconductor via near-field coupling, we deal with the stationary solution of driven and damped oscillator. The driving force is the electric field of the incident planar wave and the damping force is the near-field energy transfer described by the $\frac{1}{\tau_3^{(2)}}$ (assuming that this dissipation channel is dominating). The resulting redshifted resonance with simultaneously reduced amplitude allows for the accommodation to the balance of energy transfer to the semiconductor with incident photon energy. The amplitude of resonant plasmon oscillations $D_0(\omega)$ is thus shaped by $f(\omega)=\frac{1}{\sqrt{(\omega_1^2-\omega^2)^2+4\omega^2/(\tau_3^{(2)})^2}}$. The extremum of redshifted resonance is attained at $\omega_m=\omega_1\sqrt{1-2(\omega_1\tau_3^{(2)})^{-2}}$ with corresponding amplitude $\sim\tau_3^{(2)}/(2\sqrt{\omega_1^2-(\tau_3^{(2)})^{-2}})$. This shift is proportional to $1/\{\omega_1[\tau_3^{(2)}]^2\}$ and scales with nanosphere radius a similarly (diminishes with decreasing a) as in the experimental observations[7] [note again that for $1/\tau_1^{(2)}$ the dependence on a is opposite (grows with decreasing a)].

In order to compare with the experiment let us estimate the photocurrent in the case of a metallically modified surface in relation to the ordinary photoeffect. The photocurrent is given by $I'=|e|N(q+q_m)A$, where N is the number of incident photons and q and q_m are the probabilities of single photon attenuation in the ordinary photoeffect,[38] and in that one enhanced due to the presence of metallic nanospheres, i.e., of $q=\frac{2\sqrt{2}}{3\pi^6}\frac{e^2\mu^{5/2}}{m_p^{*2}\omega\varepsilon\hbar^3}(\hbar\omega-E_g)^{3/2}$ (cf. Ref. 38) and q_m given by Eq. (27); $A=\frac{\tau_f^n}{t_n}+\frac{\tau_f^p}{t_p}$ is the amplification factor [$\tau_f^{n(p)}$ is the annihilation time of both sign carriers, $t_{n(p)}$ is the drive time for carriers (the time of traversing the distance between electrodes)]. From the above formulas, it follows that [here $I=I'(q_m=0)$, i.e., the photocurrent without metallic modifications]

$$\frac{I'}{I}=1+7.95\times 10^5 c_0\frac{m_p^*}{m_n^*}\left[\frac{2a}{100[1\ \mathrm{nm}]}\sqrt{\frac{\hbar\omega_1[\mathrm{eV}]}{x}\left(\frac{m_p^*}{m}+\frac{m_n^*}{m}\right)}\right]^3\phi(x),\tag{28}$$

where $c_0=\frac{4\pi a^3}{3}\beta\frac{n_s}{H}$, with n_s as the surface density of metallic nanospheres, H as the semiconductor layer depth, $\phi(x)=\frac{x^2}{(x^2-1)^2+4x^2/x_1^2}\frac{1}{\sqrt{x-x_g}}$, $x=\omega/\omega_1$, $x_1=\tau_3^{(2)}\omega_1$, $x_g=E_g/(\hbar\omega_1)$, $\hbar\omega_1=2.72$ eV, and $m_{n(p)}$ as the effective mass of conduction band and valence band carriers [for Si, $m_n^*=0.19(0.98)m$, and $m_p^*=0.16(0.52)m$, for light (heavy) carriers, band gap $E_g=1.14$ eV, $\varepsilon=12$), m as the bare electron mass.

The results are summarized in Table II and in Fig. 2, for various radii of the nanospheres, and reproduce well the experimental behavior reported in Ref. 7. By x_m we denote the frequencies corresponding to the maximum value of the photocurrent (i.e., to the maximum of I'/I) (the best coincidence with the experimental data is attained at $\beta=28\times 10^{-3}\frac{50^2}{(a[\mathrm{nm}])^2}$).

In Fig. 2, an estimation of normalized photocurrent, I'/I, with respect to the wavelength is presented for three sizes of metallic nanospheres (Au) deposited on a photoactive Si layer, with various structure parameters (the proximity parameter $\beta=28\times 10^{-3}\frac{50^2}{(a[\mathrm{nm}])^2}$).

As indicated above, the relatively high value of $\frac{q_m}{q}\sim 10^4\frac{\beta 40}{H[\mathrm{nm}]}$ enables a significant growth of the efficiency of the photoenergy transfer to the semiconductor, mediated by surface plasmons in nanoparticles deposited on the active layer, by increasing β or reducing H (at constant n_s). However, because of the fact that an enhancement of β easily

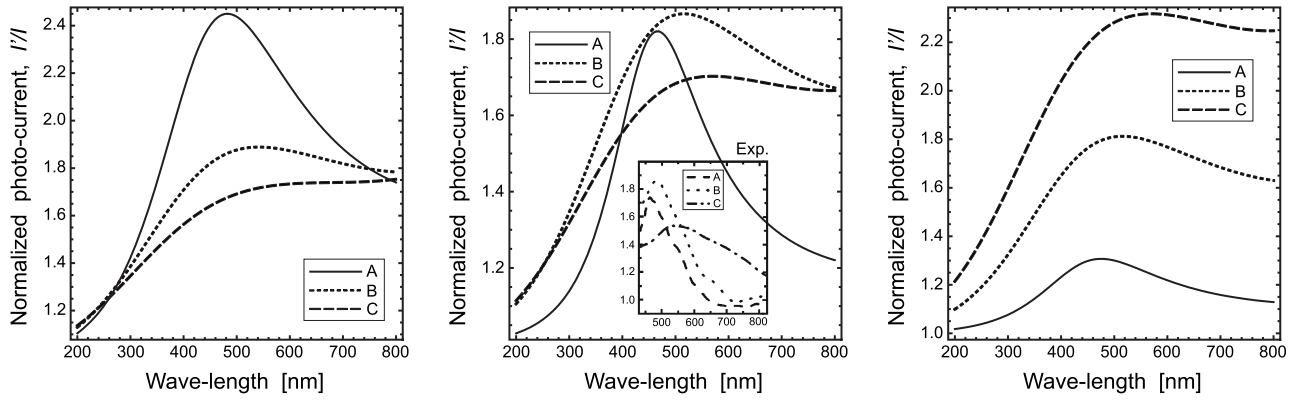

FIG. 2. Normalized photocurrent $\frac{I'}{I}(\lambda)$ for various parameters (Ref. 7): $\beta=28\times10^{-3}\frac{50^2}{(a[nm])^2}$, (left panel) $H=3$ μm, (A) $a=25$ nm, (B) 40 nm, and (C) 50 nm, with densities (A) $n_s=6.6$, (B) 1.6, and (C) $0.8\times10^8/\mathrm{cm}^2$, (central panel) $H=55$ μm, (A) $a=19$ nm, (B) 40 nm, and (C) 50 nm, with densities (A) $n_s=6.6$, (B) 1.6, and (C) $0.8\times10^8/\mathrm{cm}^2$, (right panel) $H=230$ μm, (A) $a=25$ nm, (B) 40 nm, and (C) 50 nm, with densities (A) $n_s=1.5$, (B) 1.5, and (C) $1.5\times10^8/\mathrm{cm}^2$, respectively; coincidence with the experimental data (Ref. 7) is achieved in the central panel; the inset reproduces the experimental data (Ref. 7).

induces the overdamped regime, cf. Eq. (B9), a greater perspective would be thus lowering H, the layer depth [cf. Fig. 2 (left), where a significant growth of the photocurrent with the lowering of the active layer depth H illustrates the surface character of the effect]. The overall behavior of $I'/I(\omega)=1+q_m/q$ calculated according to the relation (28), and depicted in the central panel in Fig. 2, agrees quite well with the experimental observations presented in Fig. 4 of Ref. 7 (cf. inset in the central panel of Fig. 2), in the position, height, and shape of the photocurrent curves for distinct samples (the strongest enhancement is achieved for $a=40$ nm, as indicated in the central panel of Fig. 2), though q_m/q is probably overestimated as the q denominator would be greater for a doped real semiconductor structure but was not taken into account in the present calculus, similarly as surface effects; all of these would change the q denominator as well as its energy dependence, especially for longer wavelengths, where the discrepancy between the theoretical model and the experimental data is noticeable.

IV. COMMENTS AND CONCLUSIONS

The presented analysis featuring a semiclassical RPA-type approach to collective fluctuations in large metallic nanospheres in jellium model deals with two types of plasmons, surface, and volume ones. Within this approximation the self-frequencies of surface plasmon modes are independent of the sphere radius (similarly to the classical Mie frequency for dipole surface oscillations). There are, however, also surface modes induced by the volume modes and the frequencies of these volume-induced surface oscillations depend on the sphere radius, similarly as the self-frequencies of the volume plasmons [given by the dispersion relation $\omega_{nl}^2=\omega_p^2[1+x_{nl}^2/(k_Ta^2)]$, x_{nl}—nodes of the lth spherical Bessel function]. The e-m response of the sphere consists of both resonance types, the surface, and the volume ones. It should be, however, emphasized that the excitation of the volume modes is limited by the nanoscale of the system resulting in almost uniform e-m wave fields for resonant wavelength (dipole approximation regime, as the resonant wavelength is of order of 500 nm). The dynamic electric field, uniform within the sphere, does excite the surface plasmons but not the radius-dependent volume modes. Therefore, one can conclude that the experimentally observed significant dependence of resonant e-m frequencies on the radius of nanoparticles[7] should be addressed to more complicated phenomena than radius-dependent volume modes.

The shift of the resonance frequency (in particular, for Mie dipole-type oscillations) for ultrasmall clusters (up to $a\sim2$ nm) was analyzed against various quantum effects in microscopic-type approaches, mainly of TDLDA-type[12,14,16] and also within semiclassical approaches.[13] All of these investigations indicate a major component of the experimentally observed redshift of Mie frequency due to the quantum spill-out effect (via reducing the density of electrons, resulting in factor $\sqrt{1-\frac{\Delta N}{N_e}}$ for resonance frequency, where the spill-out volume ΔN, i.e., the number of electrons outside the jellium edge, was the subject of various microscopic estimations[12–14,16]). Described in that manner, the redshift of the resonance turns out, however, to be insufficient in comparison to experimental data[13,14,17] even for small and ultrasmall clusters, and completely fails in comparison with observed shift for nanospheres with radii >10 nm (Refs. 7, 12, and 13) (for large nanospheres the pronounced redshift of surface plasmon resonance sharply grows with the sphere radius, oppositely to contribution due to spill-out in small clusters).

Note that the contribution to the redshift, though rather important in the case of small clusters, was also obtained due to the decay of plasmons for particle-hole pairs (Landau damping),[15,17] which improved fitting with the experiment, but only for ultrasmall clusters. Additionally, an opposite blueshift due to a multiplasmon anharmonic contribution was predicted.[20]

The quantum spill-out, Landau damping and coupling to ion excitations (beyond the jellium model), though important for small clusters, are thus rather weak for large nanospheres and contribute to resonance shift, for radius ranges above 10 nm, in a far lower amount than experimentally observed. In

the present paper we argue that the radius dependent shift of the plasmon resonance frequencies in large nanospheres is connected with the different factor—namely, with the interaction of surface plasmons with other components of the system, which leads to the damping of these oscillations. A damping-induced shift of the resonance for driven and damped oscillator depends on the attenuation rate, which scales with the nanosphere radius. We have analyzed various channels of surface plasmon damping. Inclusion of irradiation losses due to Lorentz friction of oscillating electrons gives the satisfactory explanation of the scale and radius dependence of plasmon resonance in metallic spheres with the radii >10 nm. The most effective channel for the surface plasmon damping turns out to be the dipole-type near-field coupling of the surface dipole plasmons with semiconductor substrate, on which metallic nanospheres would be deposited, e.g., in nanomodified diode-type systems. Due to the nanoscale of the spheres for this coupling the momentum is not conserved, which results in a strong enhancement of the interband transition probability (because all indirect electron transitions between the valence and conductivity bands in the substrate semiconductor have to be accounted for, provided energy conservation alone). This agrees with the experimental data referring to a significant growth of the energy transfer from surface plasmons in metallic nanoparticles to the semiconductor substrate.

In order to include the damping of surface plasmons one can introduce a phenomenological damping factor τ (attenuation time) to the oscillation semiclassical RPA equation for electron local density fluctuations. As the form of the resulting equation is of the damped oscillator type, thus attenuation causes a redshift in the resonance frequency, $\omega' = \sqrt{\omega^2 - \frac{1}{\tau^2}}$. For driven and damped stationary oscillations, the redshift of a resonance takes place with a maximal amplitude at $\omega_m = \sqrt{\omega^2 - \frac{2}{\tau^2}}$. This redshift is dependent on the sphere radius, via the radius dependence of τ.

The energy transfer to semiconductor surroundings mediated by surface plasmons is so effective that it may easily cause an overdamped regime for plasmon oscillations. This channel is, however, reduced (typically by 3 orders in magnitude) by proximity constraints. Nevertheless, for nanospheres deposited on the semiconductor surface, even only a small fraction of the near-field channel ($\sim \frac{h^2}{a^2} \sim 10^{-3}$, for $a \sim 50$ nm, h is an effective range of the near-field coupling) causes a strong damping of plasmons. In the case where the nanospheres are embedded in a semiconductor medium, the plasmon system would have to fall in the overdamped regime ($\omega_1 \tau \geq 1$).

In the case of a small contact of the metallic nanospheres with the semiconductor substrate or in the case of an absence of semiconductor surroundings, a significant contribution to plasmon attenuation is due to far-field radiation and electron scattering effects. The radiation contributions to $\frac{1}{\tau}$ scale with particle radius a as a^3 (for both far- and near-field channels, though in the latter case the proximity constraints, included in β, would modify this dependence to the linear one) while for scattering contribution, $\frac{1}{\tau} \sim \frac{1}{a}$. Thus, the total attenuation rate is $\frac{1}{\tau} \sim Aa^3 + Ba + C\frac{1}{a}$ (A, B, C constants). For relatively big spheres ($a > 10$ nm) the radiation channels prevail while for smaller ones the scatterings would also be important.[35,36]

The reported strengthening of photovoltaic effects due to plasmonic concentrators (layer of metallic nanoparticles on an active semiconductor surface with n_s on the order of $10^8 - 10^{10}/\mathrm{cm}^2$), for instance, up to a 20-fold increase in photocurrent in Si with nanoparticles Ag (40 nm [twofold increase], 66 nm [eightfold], and 108 nm [20-fold]),[6] indicate the significant role of the near-field energy transfer growing with the sphere radius. Other observations also confirm the strengthening role of plasmonic oscillations for the emission and absorption phenomena in semiconductor diode systems, e.g., ninefold increase in emission from an Si diode modified with Ag nanoparticles of elliptical shape 120×60 nm^2, and the resonant emission shift after covering Ag nanoparticles with a 30-nm layer of ZnS (Refs. 9 and 10) and up to 14-fold increase in absorption with various metal nanoparticles: Ag (12 nm [threefold]), Au (10 nm [fivefold]), and Cu (10 nm [14-fold]).[8] The influence of the dielectric coating is caused by the surface self-oscillation sensitivity to dielectric surroundings (as for metallic nanospheres embedded in a dielectric medium), $\omega_{0l} = \omega_p \sqrt{\frac{l}{2l+1}\frac{1}{\varepsilon}}$, and for typical $\varepsilon \sim 10$ it gives a strong decrease in the resonant frequencies by the factor ~ 0.3. The best correspondence with the experiment is attained for the reported strong dependence of the extinction features with respect to nanoparticle size (located on the surface of Si), and the shift of the resonant peak corresponding to the change of Au nanoparticle radius, 25–50 nm (stronger extremum for 40 nm)[7] and the simultaneous enhancement of photo-current seem to be well described by our model.

Some experimental data indicate, however, the existence of competitive mechanisms. For instance, for active medium TiO_2, the photocurrent diminishes in a wide spectral region (excluding the UV range) for coverings with Ag nanoparticles (3–6 nm) while the same coverings on optically active organic medium (dye solar cell) lead to a strong increase in the photocurrent for 3-nm Ag particles but to a decrease of photocurrent for 6-nm Ag particles.[9] The competitive factors can be linked here with the retardation of the carrier transfer, despite plasmonic strengthening, or with the destructive modification of a photosensitive substrate material caused by nanoparticles that are too small (greater nanoparticles are probably more convenient[6]).

Summarizing, in the presented model nanosphere surface plasmons couple with substrate charges (band electrons in a substrate semiconductor) via photonless short range *e-m* dipole interaction with very quick timing (thus very effective)—as confirmed by the time-resolved spectroscopy measurements.[7] The strong enhancement of the efficiency results from the nanoscale-induced incommensurability, leading to all momentum-indirect interband transitions, not allowed for the interaction of band electrons with the original incident planar wave photons as in an ordinary photoeffect. The type of dipole coupling is connected here with a specific *e-m* field gauge in the vicinity of the nanosphere within the distance lower than the wavelength (thus "inside" the single photon), crucially distinct than for the planar wave (in the latter case, only the vector potential can be used, which is impossible in the former case).[34] The above schematically described scenario qualitatively fits with the experimentally observed behavior and elucidates the timing of the particular

steps of the energy-transfer processes, including the mediating role of metallic nanosphere surface plasmons. The relevant time rates can be estimated within the standard quantum mechanical attitude of the Fermi-golden-rule type. Thus, the above-presented RPA plasmon description supplies the convenient and simple tool for further modeling and optimization of the metallically nanomodified solar cell structures, toward the enhancement of their efficiency.

ACKNOWLEDGMENT

Supported by the Polish KBN under Project No. N N202 260734.

APPENDIX A: CALCULATION OF TIME RATE FOR THE FAR-FIELD DIPOLE-TYPE RADIATION OF NANOSPHERE SURFACE PLASMONS

In order to estimate the attenuation coefficient due to far-field radiation losses, one can consider the damping of nanosphere plasmons to be rapidly excited by switching off the uniform electric field, $E(t)=E_0[1-\Theta(t)]$. The corresponding oscillations of the local electron density can be described by the equations

$$\frac{\partial^2 \delta\rho_1(\boldsymbol{r},t)}{\partial t^2}+\frac{2}{\tau^{(1)}}\frac{\partial \delta\rho_1(\boldsymbol{r},t)}{\partial t}=\frac{v_F^2}{3}\Delta\delta\rho_1(\boldsymbol{r},t)-\omega_p^2\delta\rho_1(\boldsymbol{r},t) \tag{A1}$$

for $r<a$ and

$$\frac{\partial^2 \delta\rho_2(\boldsymbol{r},t)}{\partial t^2}+\frac{2}{\tau_2^{(2)}}\frac{\partial \delta\rho_2(\boldsymbol{r},t)}{\partial t}$$
$$=-\frac{2\epsilon_F}{3m}\nabla\left[\frac{3}{5}n_e+\delta\rho_2(\boldsymbol{r},t)\right]\hat{\boldsymbol{r}}\delta(a+\epsilon-r)$$
$$-\left\{\frac{2\epsilon_F}{3m}\hat{\boldsymbol{r}}\nabla\ \delta\rho_2(\boldsymbol{r},t)+\frac{\omega_p^2}{4\pi}\hat{\boldsymbol{r}}\nabla\int d^3r_1\frac{1}{|\boldsymbol{r}-\boldsymbol{r}_1|}\right.$$
$$\times\left[\Theta(a-r_1)\delta\rho_1(\boldsymbol{r}_1,t)+\frac{1}{\varepsilon}\Theta(r_1-a)\delta\rho_2(\boldsymbol{r}_1,t)\right]$$
$$\left.-\frac{en_e}{m}E_r(t)\right\}\delta(a+\epsilon-r) \tag{A2}$$

for $r=a$, $(\epsilon\to 0)$. For E not dependent on r, the driving force $E(t)$ enters the second equation only and leads to the driven oscillator solution corresponding to the dipole surface plasmon oscillations $\delta\rho_2=Y_{10}(\Omega)q_{10}(t)$. Similarly, one can conclude that for nanospheres the visible light does not excite nanosphere volume plasmons as within the dipole approximation the incident wave electric field is uniform all over the sphere, unless the dipole approximation does not hold (i.e., when $a\sim\lambda$).

For $E(t)=E_0[1-\Theta(t)]$ (the rapid switching off the constant electric field E_0) the solution of Eq. (A2) has the form

$$q_{10}(t)=\sqrt{\frac{4\pi}{3}}\frac{en_e}{m\omega_1^2}E_0\begin{cases}1, & \text{for } t<0,\\ \left[\cos(\omega_1' t)+\dfrac{\sin(\omega_1' t)}{\omega_1'\tau_2^{(2)}}\right]e^{-t/\tau_2^{(2)}}, & \text{for } t\geq 0,\end{cases} \tag{A3}$$

where $\omega_1'=\sqrt{\omega_1^2-(\frac{1}{\tau_2^{(2)}})^2}$ and $\omega_1=\omega_p\sqrt{\frac{1}{3\varepsilon}}$ is the undamped dipole self-frequency.

It is easy to calculate the loss of the total energy of the system $\mathcal{A}=\mathcal{E}(t=0)-\mathcal{E}(t=\infty)$, i.e., by taking into account both the kinetic and potential energies of electron system. Only the potential interaction energy of oscillating electrons contributes, and $\mathcal{E}(t)=\text{const.}+\frac{e^2}{2\varepsilon}a^3q_{10}^2(t)$ [the time dependent part of the energy is caused by the interaction of excited electrons, $\frac{q_{10}^2(t)e^2}{2\varepsilon}\int d^3r_1,d^3r_2\frac{Y_{10}(\Omega_1)\delta(a+\epsilon_1-r_1)Y_{10}(\Omega_2)\delta(a+\epsilon_2-r_2)}{|\boldsymbol{r}_1-\boldsymbol{r}_2|}$ with $\epsilon_1,\epsilon_2\to 0$, $\epsilon_1>\epsilon_2$]. For q_{10} given Eq. (A3) one can find

$$\mathcal{A}=\mathcal{E}(t=0)-\mathcal{E}(t=\infty)=\frac{e^2}{2\varepsilon}a^3\left(\frac{4\pi}{3}\right)^2\left(\frac{en_eE_0}{m\omega_1^2}\right)^2 \tag{A4}$$

since $\mathcal{E}(t)=\text{const.}+\frac{e^2}{2\varepsilon}(\frac{4\pi}{3})^2a^3(\frac{en_eE_0}{m\omega_1^2})^2(\cos\ \omega_1' t+\frac{\sin\ \omega_1' t}{\omega_1'\tau_2^{(2)}})^2e^{-2t/\tau_2^{(2)}}$.

On the other hand, assuming that the damping of oscillations is caused by far-field radiation, one can calculate the energy loss $\mathcal{A}$ using the Poynting vector $\boldsymbol{\Pi}=\frac{c}{4\pi}\boldsymbol{E}\times\boldsymbol{B}$, $(\mu=1,\ v=\frac{c}{\sqrt{\varepsilon}})$. The scalar potential of the *e-m* wave emitted by the surface plasmon dipole oscillations: $\rho(\boldsymbol{r},t)=eq_{10}(t)Y_{10}(\Omega)\delta(a+\epsilon-r)$ is of the retarded form,

$$\phi(\boldsymbol{R},t)=\int\frac{\rho\left(\boldsymbol{r},t-\frac{|\boldsymbol{R}-\boldsymbol{r}|}{v}\right)}{\varepsilon|\boldsymbol{R}-\boldsymbol{r}|}d^3r,$$

and for

$$R\gg a,\phi(\boldsymbol{R},t)=\frac{1}{\varepsilon Rv}\hat{\boldsymbol{n}}\cdot\frac{\partial\boldsymbol{D}\left(t-\frac{R}{v}\right)}{\partial t},$$

here $\hat{\boldsymbol{n}}=\frac{\boldsymbol{R}}{R}$ and the dipole moment $\boldsymbol{D}(t-\frac{R}{v})=\int\boldsymbol{r}\rho(\boldsymbol{r},t-\frac{R}{v})d^3r$. In our case of surface plasmon dipole oscillations

$$\boldsymbol{D}\left(t-\frac{R}{v}\right)=eq_{10}\left(t-\frac{R}{v}\right)\int\boldsymbol{r}Y_{10}(\Omega)\delta(a+\epsilon-r)d^3r$$
$$=\left[0,0,eq_{10}\left(t-\frac{R}{v}\right)\sqrt{\frac{4\pi}{3}}a^3\right]. \tag{A5}$$

Similarly, for the retarded vector potential we find $\boldsymbol{A}(\boldsymbol{R},t)$

$=\frac{1}{Rc}\frac{\partial \boldsymbol{D}(t-\frac{R}{v})}{\partial t}$, [because of $\frac{\partial \rho}{\partial t}=-\mathrm{div}\,\boldsymbol{j}(\boldsymbol{r},t)$, $\phi(\boldsymbol{R},t)$ $=-\frac{1}{\varepsilon R v}\int(\hat{\boldsymbol{n}}\cdot\boldsymbol{r})\mathrm{div}\,\boldsymbol{j}(\boldsymbol{r},t-\frac{R}{v})d^3r$ $=\frac{1}{\varepsilon R v}\hat{\boldsymbol{n}}\int\boldsymbol{j}(\boldsymbol{r},t-\frac{R}{v})d^3r$ for the sphere and due to $\mathrm{div}[\boldsymbol{j}(\hat{\boldsymbol{n}}\cdot\boldsymbol{r})]$ $=(\hat{\boldsymbol{n}}\cdot\boldsymbol{r})\mathrm{div}\,\boldsymbol{j}+\boldsymbol{j}\cdot\hat{\boldsymbol{n}}$, which gives $\frac{\partial \boldsymbol{D}(t-\frac{R}{v})}{\partial t}=\int\boldsymbol{j}(\boldsymbol{r},t-\frac{R}{v})d^3r$].

Hence, for the far-field radiation of surface plasmon dipole oscillations we have

$$\boldsymbol{B}=\mathrm{rot}\,\boldsymbol{A}=-\frac{\sqrt{\varepsilon}}{c^2R}\hat{\boldsymbol{n}}\times\frac{\partial^2\boldsymbol{D}}{\partial t^2} \tag{A6}$$

and

$$\boldsymbol{E}=-\frac{1}{c}\frac{\partial\boldsymbol{A}}{\partial t}-\nabla\phi=\frac{1}{\sqrt{\varepsilon}}\boldsymbol{B}\times\hat{\boldsymbol{n}}, \tag{A7}$$

which corresponds to the planar wave, and $\boldsymbol{\Pi}=\frac{\hat{\boldsymbol{n}}}{4\pi}\frac{|\frac{\partial^2\boldsymbol{D}}{\partial t^2}|^2\sin^2\Theta}{\varepsilon v^3R^2}$, ($\Theta$ is the angle between $\boldsymbol{D}$ and $\boldsymbol{R}$). Next, taking into account that $\frac{d\mathcal{A}}{dt}=\oint\boldsymbol{\Pi}\cdot d\boldsymbol{s}$, one can find $\mathcal{A}=\int_{R/v}^{\infty}\frac{d\mathcal{A}}{dt}dt$ $=\frac{2}{3\varepsilon v^3}\int_{R/v}^{\infty}(\frac{\partial^2 D_z(t-R/v)}{\partial t^2})^2dt$. For $D_z=e\sqrt{4\pi/3}a^3q_{10}$ as in Eq. (A5), with q_{10} given by Eq. (A3), one can find in this manner

$$\mathcal{A}=\frac{2}{3}\frac{e^2}{\varepsilon v^3}\left(\frac{4\pi}{3}\right)^2a^6\left(\frac{en_eE_0}{m\omega_1^2}\right)^2(\omega_1')^4\left[1+\left(\frac{1}{\omega_1'\tau_2^{(2)}}\right)^2\right]^2 \times\int_0^{\infty}dt\left\{1+\left[-1+\left(\frac{1}{\omega_1'\tau_2^{(2)}}\right)^2\right]\sin^2\omega_1't -\frac{2\sin\omega_1't\cos\omega_1't}{\omega_1'\tau_2^{(2)}}\right\}e^{-2t/\tau_2^{(2)}}. \tag{A8}$$

The latter integral equals $\tau_2^{(2)}/4$, which together with, $(\omega_1'\tau_2^{(2)})^2+1=(\omega_1\tau_2^{(2)})^2$, leads to the expression

$$\mathcal{A}=\frac{e^2}{6\varepsilon v^3}\left(\frac{4\pi}{3}\right)^2a^6\left(\frac{en_eE_0}{m\omega_1^2}\right)^2\omega_1^4\tau_2^{(2)}. \tag{A9}$$

Via a comparison with Eq. (A4), we finally find

$$\omega_1\tau_2^{(2)}=3\left(\frac{\sqrt{3}c}{a\omega_p}\right)^3. \tag{A10}$$

APPENDIX B: CALCULATION OF DAMPING TIME RATE DUE TO THE NEAR-FIELD INTERACTION OF SURFACE PLASMONS WITH THE SEMICONDUCTOR SUBSTRATE

For the near-field regime ($\lambda>R>a$, $\lambda\gg a$), the vector potential has the same form as previously for the far field since only the condition $a\gg R$ was used for its derivation,[34]

$$\boldsymbol{A}(\boldsymbol{R},t)=\frac{1}{Rc}\frac{\partial\boldsymbol{D}\left(t-\frac{R}{v}\right)}{\partial t}.$$

In the near-field region the *e-m* field is not of planar wave type and both vector and scalar potentials are needed to describe it. The scalar potential attains the form

$$\phi(\boldsymbol{R},t)=-\,\mathrm{div}\frac{\boldsymbol{D}\left(t-\frac{R}{v}\right)}{\varepsilon R}$$

(due to the Lorentz gauge condition,[34] $\mathrm{div}\,\boldsymbol{A}=-\frac{\varepsilon\partial\phi}{c\partial t}$). The resulting Fourier components of fields $\boldsymbol{B}_\omega$ and $\boldsymbol{E}_\omega$ (i.e., for monochromatic $\boldsymbol{D}=\boldsymbol{D}_0e^{-i\omega(t-R/v)}$) can thus be represented in this case as[34]

$$\boldsymbol{B}_\omega=\frac{ik}{\sqrt{\varepsilon}}[\boldsymbol{D}_0\times\hat{\boldsymbol{n}}]\left(\frac{ik}{R}-\frac{1}{R^2}\right)e^{ikR} \tag{B1}$$

and

$$\boldsymbol{E}_\omega=\frac{1}{\varepsilon}\left\{\boldsymbol{D}_0\left(\frac{k^2}{R}+\frac{ik}{R^2}-\frac{1}{R^3}\right)+\hat{\boldsymbol{n}}(\hat{\boldsymbol{n}}\cdot\boldsymbol{D}_0)\left(-\frac{k^2}{R}-\frac{3ik}{R^2}+\frac{3}{R^3}\right)\right\}e^{ikR}, \tag{B2}$$

where we use the notation for the retarded argument, $i\omega(t-\frac{R}{c})=i\omega t-ikR$. For the near-field region $kR\ll1$, one can neglect terms with $\frac{1}{R}$ and $\frac{1}{R^2}$. Assuming also that for the near-field $e^{ikR}=1$, one can thus obtain $\boldsymbol{B}_\omega=0$ and that $\boldsymbol{E}_\omega$ $=\frac{1}{\varepsilon R^3}[3\hat{\boldsymbol{n}}(\hat{\boldsymbol{n}}\cdot\boldsymbol{D}_0)-\boldsymbol{D}_0]$, which corresponds to the dipole electric field.

The dipole type near-field potential can be written as follows:

$$\varphi(\boldsymbol{R},t)=\frac{1}{\varepsilon R^2}\boldsymbol{n}\cdot\boldsymbol{D}_0\sin(\omega t+\alpha)=w^+e^{i\omega t}+w^-e^{-i\omega t}, \tag{B3}$$

where $w^+=(w^-)^*=\frac{e}{\varepsilon R^2}\frac{1}{2i}e^{i\alpha}\boldsymbol{n}\cdot\boldsymbol{D}_0$; one can confine Eq. (B3) only to the w^+ term, corresponding to the energy absorption in the semiconductor. Then, according to the Fermi golden rule, the transition probability per time unit between states $\Psi_{1\boldsymbol{k}_1}(\boldsymbol{r},t)=(2\pi)^{-3/2}\exp[i\boldsymbol{k}_1\cdot\boldsymbol{r}-iE_1(\boldsymbol{k}_1)t/\hbar]$, $\Psi_{2\boldsymbol{k}_2}(\boldsymbol{r},t)$ $=(2\pi)^{-3/2}\exp[i\boldsymbol{k}_2\cdot\boldsymbol{r}-iE_2(\boldsymbol{k}_2)t/\hbar]$ (semiconductor electron states from the valence and conduction bands, respectively) equals

$$w(\boldsymbol{k}_1,\boldsymbol{k}_2)=\frac{2\pi}{\hbar}|\langle\boldsymbol{k}_1|w^+|\boldsymbol{k}_2\rangle|^2\delta[E_1(\boldsymbol{k}_1)-E_2(\boldsymbol{k}_2)+\hbar\omega], \tag{B4}$$

where $\langle\boldsymbol{k}_1|w^+|\boldsymbol{k}_2\rangle=\frac{1}{(2\pi)^3}\int\frac{e}{\varepsilon 2i}e^{i\alpha}\boldsymbol{n}\cdot\boldsymbol{D}_0\frac{e^{-i(\boldsymbol{k}_1-\boldsymbol{k}_2)\cdot\boldsymbol{R}}}{R^2}d^3R$. Taking the z axis along the vector $\boldsymbol{q}=\boldsymbol{k}_2-\boldsymbol{k}_1$, then $\boldsymbol{q}\cdot\boldsymbol{R}=qR\cos\Theta_1$, $\boldsymbol{n}\cdot\boldsymbol{D}_0=D_0(\cos\Theta\cos\Theta_1+\sin\Theta\sin\Theta_1\cos\phi_1)$ (Θ is an angle between $\boldsymbol{D}_0$ and $\boldsymbol{q}$). Hence,

$$\langle\boldsymbol{k}_1|w^+|\boldsymbol{k}_2\rangle=\frac{e}{(2\pi)^3 2i\varepsilon}e^{i\alpha}D_0\int_0^{\infty}dR\int_0^{\pi}\sin\Theta_1d\Theta_1\int_0^{2\pi}d\phi_1 \times[\cos\Theta\cos\Theta_1+\sin\Theta\sin\Theta_1\cos\phi_1]e^{iqR\cos\Theta_1} =\frac{eD_0}{(2\pi)^2\varepsilon}e^{i\alpha}\frac{\cos\Theta}{q},$$

(as $\int_0^{\pi}\cos\Theta_1\sin\Theta_1d\Theta_1e^{ix\cos\Theta_1}=-i\frac{d}{dx}2\frac{\sin x}{x}$) and the probability of transition $w(\boldsymbol{k}_1,\boldsymbol{k}_2)=\frac{e^2D_0^2}{(2\pi)^3\hbar\varepsilon^2}\frac{\cos^2\Theta}{q^2}\delta[E_1(\boldsymbol{k}_1)-E_2(\boldsymbol{k}_2)+\hbar\omega]$. In order to include all possible initial and final states in the semiconductor, the summation with respect to $\boldsymbol{k}_1$ and

$\boldsymbol{k}_2$ has to be performed [including filling factors $f(\boldsymbol{k}_1)\simeq 1$ and $f(\boldsymbol{k}_2)\simeq 0$, as well as the absorption and emission of energy]. In the result, we arrive with the total transition probability in the semiconductor per time unit $\delta w \simeq \int \frac{d^3k_1}{4\pi^3}\int \frac{d^3k_2}{4\pi^3} w(\boldsymbol{k}_1,\boldsymbol{k}_2)$ caused by dipole surface plasmon oscillations on the single nanosphere.

Let us emphasize that due to the absence of the momentum conservation for the near-field dipole coupling in the vicinity of the nanosphere, all interband transitions contribute, not only direct ones (as for the interaction with the planar wave). This results in the strong enhancement of the transition probability for the near-field coupling in comparison to the photon (planar waves) attenuation rate in a semiconductor in an ordinary photoeffect.

For the simplest model band structure, $E_1(\boldsymbol{k}_1)-E_2(\boldsymbol{k}_2)+\hbar\omega=x+y-\gamma$, where $x=\frac{\hbar^2k_1^2}{2m_p^*}$, $x=\frac{\hbar^2k_2^2}{2m_n^*}$, and $\gamma=\hbar\omega-E_g$ (E_g is the semiconductor band gap), the integration over the wave vectors gives the formula for the total probability of the transition

$$\delta w = \frac{e^2D_0^2\mu\sqrt{m_p^*m_n^*}}{3(4\pi^3)^2\hbar^5\varepsilon^2}(\hbar\omega_1-E_g), \tag{B5}$$

where $\mu=\frac{m_p^*m_n^*}{m_p^*+m_n^*}$.

Assuming now that the dipole plasmon oscillations correspond to the damped oscillations that were excited by the rapid switching off of the uniform electric field (as in the Appendix A), $E(t)=E_0[1-\Theta(t)]$, with the dipole-type solution for electron distribution given by Eq. (A3), we have

$$\boldsymbol{D}(t)=[0,0,D_0e^{-t/\tau_3^{(2)}}\cos(\omega_1't)] \tag{B6}$$

with

$$D_0=\frac{e^2n_e}{m\omega_1^2}E_0\frac{4\pi}{3}a^3 \tag{B7}$$

in comparison to Eq. (A3) we have neglected here the second term $\frac{\sin(\omega_1't)}{\omega_1'\tau_3^{(2)}}$ for $\tau_3^{(2)}\omega_1'$ well greater than unity.

One can now estimate the total energy transfer to the semiconductor (assuming that the dominant channel of the dissipation is the near-field interaction with the semiconductor substrate and neglecting here the small shift of ω_1' due to dissipation)

$$\begin{aligned}\mathcal{A}&=\beta\int_0^\infty \delta w\hbar\omega_1 dt\\ &=\beta\hbar\omega_1\delta w\tau_3^{(2)}/2\\ &=\beta\frac{\mu e^6n_e^2E_0^2a^6\tau_3^{(2)}\sqrt{m_n^*m_p^*}\hbar\omega_1(\hbar\omega_1-E_g)}{6(3\pi^2)^2m^2\omega_1^4\hbar^5\varepsilon^2},\end{aligned} \tag{B8}$$

where β accounts for the proximity constraints that reduce the near-field contact of the sphere with the semiconductor medium; for the case of nanospheres deposited on the semiconductor layer surface $\beta\sim\frac{h^2}{a^2}\sim 10^{-3}$, for $a\sim 50$ nm (h is an effective range of the near-field coupling) while for the nanospheres entirely embedded in the semiconductor surroundings β would enhance significantly. Comparing the value given by the formula (B8) with the energy loss given by Eq. (A4) one can find

$$\frac{1}{\tau_3^{(2)}\omega_1}=\beta\frac{e^2a^3\mu\sqrt{m_n^*m_p^*}(\hbar\omega_1-E_g)}{48\pi^6h\hbar^4\varepsilon}. \tag{B9}$$

For nanospheres of Au deposited on the Si layer we obtain

$$\frac{1}{\tau_3^{(2)}\omega_1}=0.00071\beta\left(\frac{a}{[1\ \text{nm}]}\right)^3\frac{\mu}{m}\frac{\sqrt{m_n^*m_p^*}}{m}, \tag{B10}$$

for light (heavy) carriers in Si, $m_n=0.19(0.98)m$, $m_p=0.16(0.52)m$, and $E_g=1.14$ eV, $\varepsilon=12$, and $\hbar\omega_1=2.72$ eV.

[1] W. L. Barnes, A. Dereux, and T. W. Ebbesen, Nature (London) **424**, 824 (2003).
[2] A. V. Zayats, I. I. Smolyaninov, and A. A. Maradudin, Phys. Rep. **408**, 131 (2005).
[3] S. A. Maier, *Plasmonics: Fundamentals and Applications* (Springer, Berlin, 2007).
[4] S. Pillai, K. R. Catchpole, T. Trupke, G. Zhang, J. Zhao, and M. A. Green, Appl. Phys. Lett. **88**, 161102 (2006).
[5] M. Westphalen, U. Kreibig, J. Rostalski, H. Lüth, and D. Meissner, Sol. Energy Mater. Sol. Cells **61**, 97 (2000); M. Gratzel, J. Photochem. Photobiol. C **4**, 145 (2003).
[6] H. R. Stuart and D. G. Hall, Appl. Phys. Lett. **73**, 3815 (1998); H. R. Stuart and D. G. Hall, Phys. Rev. Lett. **80**, 5663 (1998); H. R. Stuart and D. G. Hall, Appl. Phys. Lett. **69**, 2327 (1996).
[7] D. M. Schaadt, B. Feng, and E. T. Yu, Appl. Phys. Lett. **86**, 063106 (2005).
[8] K. Okamoto, I. Niki, A. Shvartser, Y. Narukawa, T. Mukai, and A. Scherer, Nature Mater. **3**, 601 (2004); K. Okamoto, I. Niki, A. Scherer, Y. Narukawa, T. Mukai, and Y. Kawakami, Appl. Phys. Lett. **87**, 071102 (2005).
[9] C. Wen, K. Ishikawa, M. Kishima, and K. Yamada, Sol. Energy Mater. Sol. Cells **61**, 339 (2000).
[10] P. Lalanne and J. P. Hugonin, Nat. Phys. **2**, 551 (2006).
[11] G. Mie, Ann. Phys. **25**, 329 (1908).
[12] M. Brack, Rev. Mod. Phys. **65**, 677 (1993).
[13] V. V. Kresin, Phys. Rep. **220**, 1 (1992).
[14] W. Ekardt, Phys. Rev. B **31**, 6360 (1985).
[15] W. Ekardt, Phys. Rev. B **33**, 8803 (1986).
[16] G. Weick, R. A. Molina, D. Weinmann, and R. A. Jalabert, Phys. Rev. B **72**, 115410 (2005).
[17] G. Weick, G. L. Ingold, R. A. Jalabert, and D. Weinmann, Phys. Rev. B **74**, 165421 (2006); C. Yannouleas, R. A. Broglia, M. Brack, and P. F. Bortignon, Phys. Rev. Lett. **63**, 255 (1989).
[18] L. Serra, F. Garcias, M. Barranco, N. Barberan, and J. Navarro, Phys. Rev. B **41**, 3434 (1990).
[19] A. Rubio and L. Serra, Phys. Rev. B **48**, 18222 (1993).

[20] L. G. Gerchikov, C. Guet, and A. N. Ipatov, Phys. Rev. A **66**, 053202 (2002).
[21] W. Ekardt, Phys. Rev. Lett. **52**, 1925 (1984).
[22] C. F. Bohren and D. R. Huffman, *Absorption and Scattering of Light by Small Particles* (Wiley, New York, 1983).
[23] U. Kreibig and M. Vollmer, *Optical Properties of Metal Clusters* (Springer, Berlin, 1995).
[24] M. Brack, Phys. Rev. B **39**, 3533 (1989).
[25] A. B. Migdal, J. Phys. (USSR) **8**, 331 (1944).
[26] H. von Steinwedel and J. H. D. Jensen, Z. Naturforsch. A **5**, 413 (1950).
[27] M. Goldhaber and E. Teller, Phys. Rev. **74**, 1046 (1948).
[28] D. Pines, *Elementary Excitations in Solids* (ABP Perseus Books, Massachusetts, 1999).
[29] D. Pines and D. Bohm, Phys. Rev. **85**, 338 (1952); D. Bohm and D. Pines, *ibid.* **92**, 609 (1953).
[30] W. Jacak, J. Krasnyj, J. Jacak, R. Gonczarek, A. Chepok, L. Jacak, D. Hu, and D. Schaadt, J. Appl. Phys. **107**, 124317 (2010).
[31] J. I. Petrov, *Physics of Small Particles* (Nauka, Moscow, 1984).
[32] M. L. Brongersma, J. W. Hartman, and H. A. Atwater, Phys. Rev. B **62**, R16356 (2000).
[33] B. Lambrecht, A. Leitner, and F. R. Aussenegg, Appl. Phys. B: Lasers Opt. **64**, 269 (1997).
[34] L. D. Landau and E. M. Lifshitz, *Field Theory* (Nauka, Moscow, 1973).
[35] F. Stietz, J. Bosbach, T. Wenzel, T. Vartanyan, A. Goldmann, and aF. Träger, Phys. Rev. Lett. **84**, 5644 (2000).
[36] M. Scharte, R. Porath, T. Ohms, M. Aeschlimann, J. R. Krenn, H. Ditlbacher, F. R. Aussenegg, and A. Liebsch, Appl. Phys. B: Lasers Opt. **73**, 305 (2001).
[37] U. Kreibig and L. Genzel, Surf. Sci. **156**, 678 (1985).
[38] P. S. Kiriejew, *Physics of Semiconductors* (PWN, Warsaw, 1969).